ARTHRITIS & RHEUMATOLOGY
Vol. 70, No. 5, May 2018, pp 690–701
DOI 10.1002/art.40428

Identification of Three Rheumatoid Arthritis Disease Subtypes by Machine Learning Integration of Synovial Histologic Features and RNA Sequencing Data

Dana E. Orange,[1] Phaedra Agius,[2] Edward F. DiCarlo,[3] Nicolas Robine,[2] Heather Geiger,[2] Jackie Szymonifka,[3] Michael McNamara,[3] Ryan Cummings,[3] Kathleen M. Andersen,[3] Serene Mirza,[3] Mark Figgie,[3] Lionel B. Ivashkiv,[3] Alessandra B. Pernis,[3] Caroline S. Jiang,[4] Mayu O. Frank,[5] Robert B. Darnell,[5] Nithya Lingampali,[6] William H. Robinson,[6] Ellen Gravallese,[7] for the Accelerating Medicines Partnership in Rheumatoid Arthritis and Lupus Network, Vivian P. Bykerk,[3] Susan M. Goodman,[3] and Laura T. Donlin[3]

Objective. **In this study, we sought to refine histologic scoring of rheumatoid arthritis (RA) synovial tissue by training with gene expression data and machine learning.**

Methods. **Twenty histologic features were assessed in 129 synovial tissue samples (n = 123 RA patients and n = 6 osteoarthritis [OA] patients). Consensus clustering was performed on gene expression data from a subset of 45 synovial samples. Support vector machine learning was used to predict gene expression subtypes, using histologic data as the input. Corresponding clinical data were compared across subtypes.**

Results. **Consensus clustering of gene expression data revealed 3 distinct synovial subtypes, including a high inflammatory subtype characterized by extensive infiltration of leukocytes, a low inflammatory subtype characterized by enrichment in pathways including transforming growth factor β, glycoproteins, and neuronal genes, and a mixed subtype. Machine learning applied to histologic features, with gene expression subtypes serving as labels, generated an algorithm for the scoring of histologic features. Patients with the high inflammatory synovial subtype exhibited higher levels of markers of systemic inflammation and autoantibodies. C-reactive protein (CRP) levels were significantly correlated with the severity of pain in the high inflammatory subgroup but not in the others.**

Conclusion. **Gene expression analysis of RA and OA synovial tissue revealed 3 distinct synovial subtypes.**

Supported by the New York Genome Center, Rockefeller University (grant UL1-TR001866 from the National Center for Advancing Translational Sciences, NIH Clinical and Translational Science Award program), the Weill Cornell Medical Center Clinical Translational Science Center, and The Block Family Foundation. Dr. Ivashkiv's work was supported by the NIH (grant AR-046713). Dr. Donlin's work was supported by the NIH (grant KO1-AR066063). This work was also supported by the Accelerating Medicines Partnership (AMP) in Rheumatoid Arthritis and Lupus Network. AMP is a public–private partnership (AbbVie, Arthritis Foundation, Bristol-Myers Squibb, Lupus Foundation of America, Lupus Research Alliance, Merck Sharp & Dohme, NIH, Pfizer, Rheumatology Research Foundation, Sanofi, and Takeda Pharmaceuticals International) created to develop new ways of identifying and validating promising biologic targets for diagnostics and drug development. Funding was provided by the NIH (grants UH2-AR-067676, UH2-AR-067677, UH2-AR-067679, UH2-AR-067681, UH2-AR-067685, UH2-AR-067688, UH2-AR-067689, UH2-AR-067690, UH2-AR-067691, UH2-AR-067694, and UM2-AR-067678).

[1]Dana E. Orange, MD, MSc: Hospital for Special Surgery, The Rockefeller University, and New York Genome Center, New York, New York; [2]Phaedra Agius, PhD, Nicolas Robine, PhD, Heather Geiger, BA: New York Genome Center, New York, New York; [3]Edward F. DiCarlo, MD, Jackie Szymonifka, PhD, Michael McNamara, BS, Ryan Cummings, AB, Kathleen M. Andersen, BSc, Serene Mirza, BS, Mark Figgie, MD, Lionel B. Ivashkiv, MD, Alessandra B. Pernis, PhD, Vivian P. Bykerk, MD, Susan M. Goodman, MD, Laura T. Donlin, PhD: Hospital for Special Surgery, New York, New York; [4]Caroline S. Jiang, PhD: The Rockefeller University Hospital, New York, New York; [5]Mayu O. Frank, NP, PhD, Robert B. Darnell, MD, PhD: The Rockefeller University and New York Genome Center, New York, New York; [6]Nithya Lingampali, BS, William H. Robinson, MD, PhD: Stanford University School of Medicine, Stanford, California; [7]Ellen Gravallese, MD: University of Massachusetts Memorial Medical Center, Worcester.

Drs. Orange and Agius contributed equally to this work. Drs. Bykerk, Goodman, and Donlin contributed equally to this work.

Dr. DiCarlo has received consulting fees, speaking fees, and/or honoraria from Wright Medical Technologies (less than $10,000). Dr. Gravallese has received consulting fees, speaking fees, and/or honoraria from Eli Lilly and Company, Sanofi Genzyme, Celgene, and UpToDate (less than $10,000 each).

Address correspondence to Dana E. Orange, MD, MSc, The Rockefeller University, 1230 York Avenue, New York, NY 10065 (e-mail: dorange@rockefeller.edu); or to Laura T. Donlin, PhD, Hospital for Special Surgery, 535 East 70th Street, New York, NY 10021 (e-mail: DonlinL@HSS.edu).

Submitted for publication September 15, 2017; accepted in revised form January 23, 2018.

These labels were used to generate a histologic scoring algorithm in which the histologic scores were found to be associated with parameters of systemic inflammation, including the erythrocyte sedimentation rate, CRP level, and autoantibody levels. Comparison of gene expression patterns to clinical features revealed a potentially clinically important distinction: mechanisms of pain may differ in patients with different synovial subtypes.

Rheumatoid arthritis (RA) is the most prevalent autoimmune arthritis, manifested primarily as extensive inflammation in the synovial tissue leading to joint destruction. Assessment of synovium has the potential to provide guidance regarding optimal treatment strategies (1–5); however, classification of RA synovium is not yet factored into the current diagnostic criteria for RA, nor is it incorporated into current treatment guidelines (6). A hematoxylin and eosin (H&E) stain–based assessment of RA synovium is feasible for large numbers of patients undergoing interventional procedures, since it is a routine offering by clinical pathology laboratories. The Krenn scoring system of H&E-stained synovial tissue involves assessment of 3 histologic features: synovial lining hyperplasia, synoviocyte stromal density, and leukocyte infiltration (7–10). Although the presence of high-grade synovitis has a sensitivity of 62% and specificity of 96% for the diagnosis of rheumatic diseases, it does not discriminate between subtypes of rheumatic diseases, such as RA versus psoriatic arthritis.

We therefore reasoned that a more granular histologic scoring system could be useful as a tool to subtype and guide the treatment of RA. Others have explored the significance of lymphocyte aggregates and found correlations with systemic markers of inflammation, such as the erythrocyte sedimentation rate (ESR) and C-reactive protein (CRP) level, but not with factors with higher specificity, such as measurements of anti–citrullinated peptide antibodies (ACPAs) and rheumatoid factor (RF) (11), suggesting that these features alone cannot distinguish immunologically distinct subtypes of RA.

Assessments of H&E-stained slides can detect an array of inflammatory features, including multinucleated giant cells (12), neutrophils (13), plasma cells (14), binucleated plasma cells (15), and Russell bodies (enlarged plasma cells undergoing excessive synthesis of immunoglobulin) (14), as well as extracellular features such as deposition of fibrin (the final product of the clotting cascade [13]), mucins (a heterogeneous family of heavily glycosylated glycoproteins that retain water and therefore form gels in RA and osteoarthritis [OA] synovium, but not normal synovial tissue [16]), and detritus (small fragments of cartilage or bone [17]). Herein, we aimed to evaluate the relative utility of identifying 20 such features for the differentiation of synovial subtypes defined by transcriptome-wide gene expression patterns, with the goal of developing an algorithm to score histologic features in a manner that distinguishes each of the synovial subtypes.

We performed an integrative analysis of clinical, histologic, and gene expression data from a cohort of 123 RA patients and 6 OA patients, with the aim of gaining further insights into synovial tissue inflammation and the subclassification of RA. Gene expression cluster analysis identified 3 synovial subtypes, which were used as labels to train a support vector machine (SVM) learning algorithm in which scores of histologic features were utilized as the input. This analysis produced a histologic scoring algorithm that may be used to predict the 3 gene expression subtypes in RA and OA patients using only histologic features, and that corresponded to the levels of acute-phase reactants and autoantibodies in these patients.

PATIENTS AND METHODS

Patient data. An overview of the study design is presented in Figure 1. We enrolled 123 consecutive patients with RA undergoing arthroplasty at the Hospital for Special Surgery (HSS) in New York who had met either the American College of Rheumatology (ACR)/European League Against Rheumatism 2010 classification criteria for RA (18) and/or the ACR 1987 criteria for RA (19). In addition, synovial samples from 6 patients with OA were included in the analyses.

The serum status of ACPAs (measured with the anti–cyclic citrullinated peptide antibody [anti-CCP] test) and RF was coded as negative, low or medium positive (1–3 times the upper limit of normal), or high positive (>3 times the upper limit of normal). Pain was assessed by asking patients the question, "How much pain have you had because of your condition over the past week? Please indicate how severe your pain has been on a scale of 0–10." This study was approved by the HSS Institutional Review Board (approval no. 2014-233), the Rockefeller

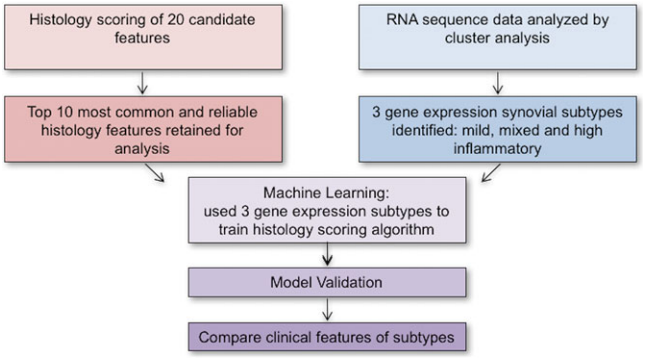

Figure 1. Study overview.

University Institutional Review Board (approval no. DOR0822), and the Biomedical Research Alliance of New York (approval no. 15-08-114-385). All participating patients provided their signed informed consent.

Sample processing. Adjacent areas of synovial tissue were placed into OCT frozen blocks for histology and processed for cell dissociation. For dissociation, the tissue was dissected and treated with Liberase TL (100 μg/ml; Roche) and DNase I (100 μg/ml; Roche) at 37°C for 15 minutes. Red blood cells were lysed and the remaining cells were washed and filtered through 70-μ*M* strainers. Synovial cells were lysed in RLT (Qiagen) with 1% β-mercaptoethanol, and then stored at −80°C.

RNA sequencing. RNA was extracted using a Qiagen RNeasy Mini kit (no. 74104). Libraries were prepared using Truseq messenger RNA (mRNA) Stranded Library kits; 50-bp, paired-end reads were sequenced on a HiSeq2500 platform. Reads were aligned to hg19 using STAR (20). Samples with >0.1% globin mRNA were excluded from further analysis to prevent confusion between infiltrating and contaminating hematopoietic cells. Forty-five samples of sufficient quality were processed in 3 separate batches. To account for any batch effects, we used ComBaT in the Bioconductor SVA package (21) and DESeq2 (22) to normalize the data.

Clustering of RNA-seq data. RNA-seq data were clustered using consensus clustering, an iterative clustering method in which small data perturbations (using the *morm* function in the basic stats package in R) are introduced at each clustering iteration. The clustering iterations offer the opportunity to derive a statistically robust data partitioning, as opposed to a one-time, single clustering computation. We used the k-means clustering method, which typically does not converge to the same solution when clustering the same data multiple times (contrary to agglomerative approaches, such as hierarchical clustering). We clustered the 45 RNA-seq samples 1,000 times into k = 2, k = 3, k = 4, and k = 5 clusters. The clustering iterations were then used to generate likelihood scores representing the frequency of a pair of samples clustering together (number of times the pair of samples cluster together divided by the number of clustering iterations). This score ranges from 0 to 1, with scores of 1 indicating co-clustering of the 2 samples.

Differential gene expression analysis. We used the DESeq2 Bioconductor package (22) to identify differentially expressed genes (DEGs) across the synovial subtypes identified via clustering, at an adjusted *P* (P_{adj}) value of 0.01. We eliminated chromosome X/Y genes to remove sex biases, as well as IgG variable (V, D, and J) genes, since the individual V-, D-, and J-gene segments are counted as individual immunoglobulin genes, thereby overrepresenting their abundance. Immunoglobulin constant regions were retained to ensure representation of immunoglobulin gene expression.

Pathway analysis. DAVID analytic modules (version 6.8) (23) with default parameters were used to identify functional annotation clusters of genes. Genes found to be differentially expressed in the high inflammatory subgroup compared to the other subgroups and low inflammatory subgroup compared to the other subgroups, with a P_{adj} value of less than 0.05 and a $\log_2$-transformed fold change of greater than 0.5, were used to identify enriched pathways. Enrichment scores were the modified *P* values from Fisher's exact test based on data from the gene-enrichment analysis.

Inference of cell types in gene expression clusters. In order to deconvolute the cellular composition of the 3 subtypes in our data, we used an algorithm called CIBERSORT (Cell-type Identification by Estimating Relative Subsets of Known RNA Transcripts) (24,25), a machine learning system trained on the profiles of 22 distinct leukocyte data sets over 547 genes, with defined "barcodes" of gene expression signatures to distinguish cell types.

Predicting RNA-seq subtypes from histologic features. We used histologic scores as modeling features in a standard SVM (Bioconductor package e1071) to predict the 3 RNA-seq subtypes, using leave-one-out cross validation to train and predict transcriptomic subtypes. Weights attributed to each feature were extracted from an SVM. All histologic features were presented as binary vectors—histologic features having more than 2 categories were converted to a binary representation, so that all features were equally represented in the model.

Histologic scoring. In total, 129 synovial samples were preferentially obtained from grossly inflamed (dull and opaque) synovium. If no inflammation was apparent, samples were obtained from standard locations: the femoral aspects of the medial and lateral gutters, and the central supratrochlear region in the suprapatellar pouch. Tissue samples were snap-frozen and stained with Harris' modified hematoxylin solution and eosin Y (both from Sigma-Aldrich). Twenty histologic features (synovial lining hyperplasia, lymphocytes, plasma cells, Russell bodies, binucleated plasma cells, fibrin, synovial lining giant cells, sublining giant cells, fibrosis, detritus, necrosis, granulation tissue, neutrophils, mast cells, eosinophils, synovial chondrometaplasia, germinal centers, mucin, infarction, and vascularity) were scored using a systematic approach (as outlined in detail in Supplementary Methods, available on the *Arthritis & Rheumatology* web site at http://onlinelibrary.wiley.com/doi/10.1002/art.40428/abstract and also available at www.hss.edu/pathology-synovitis). In total, 129 synovial samples were scored by a single pathologist (EFD), and 40 samples were scored again by a second pathologist (EG) to determine interrater reliability.

ACPA array. As previously described (24), serum levels of antibodies targeting 38 putative RA-associated autoantigens were measured using a custom bead-based immunoassay. Serum samples were diluted at a 1:30 ratio in a proprietary dilution buffer (Bio-Rad), mixed with the antigens conjugated to spectrally distinct fluorescent microspheres (Bio-Rad), and then incubated with an anti-human IgG antibody conjugated to phycoerythrin (Jackson ImmunoResearch). The resulting fluorescence intensities were quantitated using a Luminex 200 System.

Statistical analysis. Kappa statistics were used to assess the interrater reliability of the histologic scores sourced from the 2 pathologists. For variables with ≥3 response levels, weighted kappa statistics were calculated to give credit for differences that were close, as opposed to treating any difference as the same. Interrater reliability was scored as follows: none to slight, κ = 0.01–0.2; fair, κ = 0.21–0.40; moderate, κ = 0.41–0.60; substantial, κ = 0.61–0.80; and almost perfect, κ = 0.81–1.00 (25). The Jonckheere-Terpstra 2-sided test for trend was used to compare pathway enrichment scores from the gene set variation analysis data across the 3 synovial subtypes. Kruskal-Wallis test with Dunn's test for multiple comparisons was used to compare CIBERSORT RNA scores and clinical features among the 3 synovial subtypes. The chi-square test was used to detect differences in binary data above those expected by chance among the 3 synovial subtypes. Analysis of variance with Tukey's test for multiple comparisons was used to compare the $\log_2$-transformed

mean fluorescence intensities of ACPA expression among the 3 synovial subtypes. Spearman's correlation coefficients were calculated to assess correlations between the severity of pain and gene expression levels across the 3 synovial subtypes.

RESULTS

Clinical characteristics. The clinical characteristics of the 123 patients with RA are presented in Supplementary Table 1 (available on the *Arthritis & Rheumatology* web site at http://onlinelibrary.wiley.com/doi/10.1002/art.40428/abstract). The majority of the RA patients were female. Among the 123 patients, 47% were seropositive for RF and 50% were seropositive for anti-CCP. Although the mean disease duration of the RA patients was 14 years, the mean Disease Activity Score in 28 joints was 3.8 (indicative of moderate disease activity), and 53% of the patients were treated with a biologic agent just prior to surgery. The affected joints included the hips in 40% of patients, knees in 57% of patients, and shoulders in 3% of patients.

Histologic features of the extracted synovium. We first sought to determine the prevalence and feasibility of scoring the candidate histologic features of the RA and OA synovium. Fourteen of the 20 features were observed in >5% of synovial samples (Figure 2A).

We next evaluated the interrater reliability for the scoring of these histologic features on a subset of samples (Figure 2B). Representative images of the features with a frequency of >5% in the synovial samples and having at least fair interrater reliability are presented in Figures 2C and D. Features that were seen in at least 5% of samples and that had at least fair interpathologist reliability

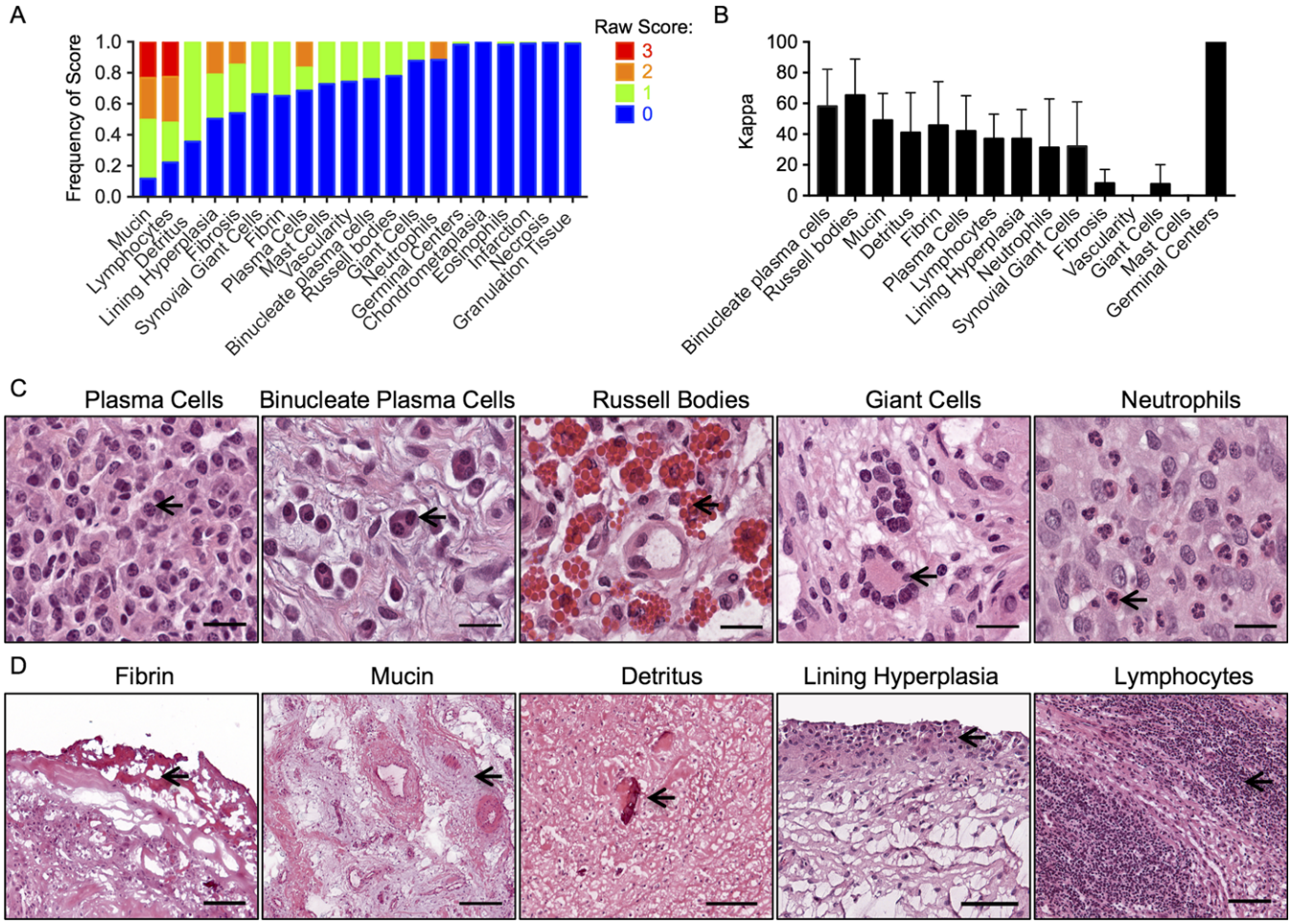

Figure 2. Histologic features of the arthritic synovium. **A,** Frequency distribution of histologic scores of 20 features assessed in 129 synovial samples from patients with rheumatoid arthritis or osteoarthritis. **B,** Interrater reliability of the assessment of 15 histologic features by 2 pathologists in 40 synovial samples. Results are the mean ± SD kappa statistic. **C** and **D,** Representative images of hematoxylin and eosin–stained synovium, showing 10 synovial histologic features (**arrows**) that were retained for modeling based on a frequency of >5% and fair interrater reliability. Original magnification × 100 (bars = 200 μm) in **C**; × 20 (bars = 20 μm) in **D**.

included plasma cells, binucleated plasma cells, Russell bodies, giant cells, neutrophils, fibrin, mucin, detritus, synovial lining hyperplasia, and lymphocytes.

Three distinct subtypes of synovium identified by RNA-seq data analysis. Independent of the histologic analysis, consensus clustering of the top 500 most variable genes expressed in the 45 synovial samples (39 from patients with RA and 6 from patients with OA) identified 3 gene expression subtypes. Figure 3A depicts the pairwise likelihood scores for the likelihood of samples clustering together, with the 45 samples being constrained to k = 2, k = 3, and k = 4 clusters. The red boxes in Figure 3A represent the co-clustering samples (likelihood scores of 1), blue represents the samples that never co-clustered (scores of 0), and white represents inconsistent co-clustering patterns (scores of 0.5). When the samples were partitioned into 2 or 3 clusters, the likelihood score was crisp and well defined, with the sharp red and blue colors suggesting that the majority of the likelihood scores approached 1 or 0. However, when the samples were clustered into 4 or more groups, significantly less consistency was observed. This visualization is a statistically robust confirmation that the 45 RNA-seq samples formed, at most, 3 distinct subgroups.

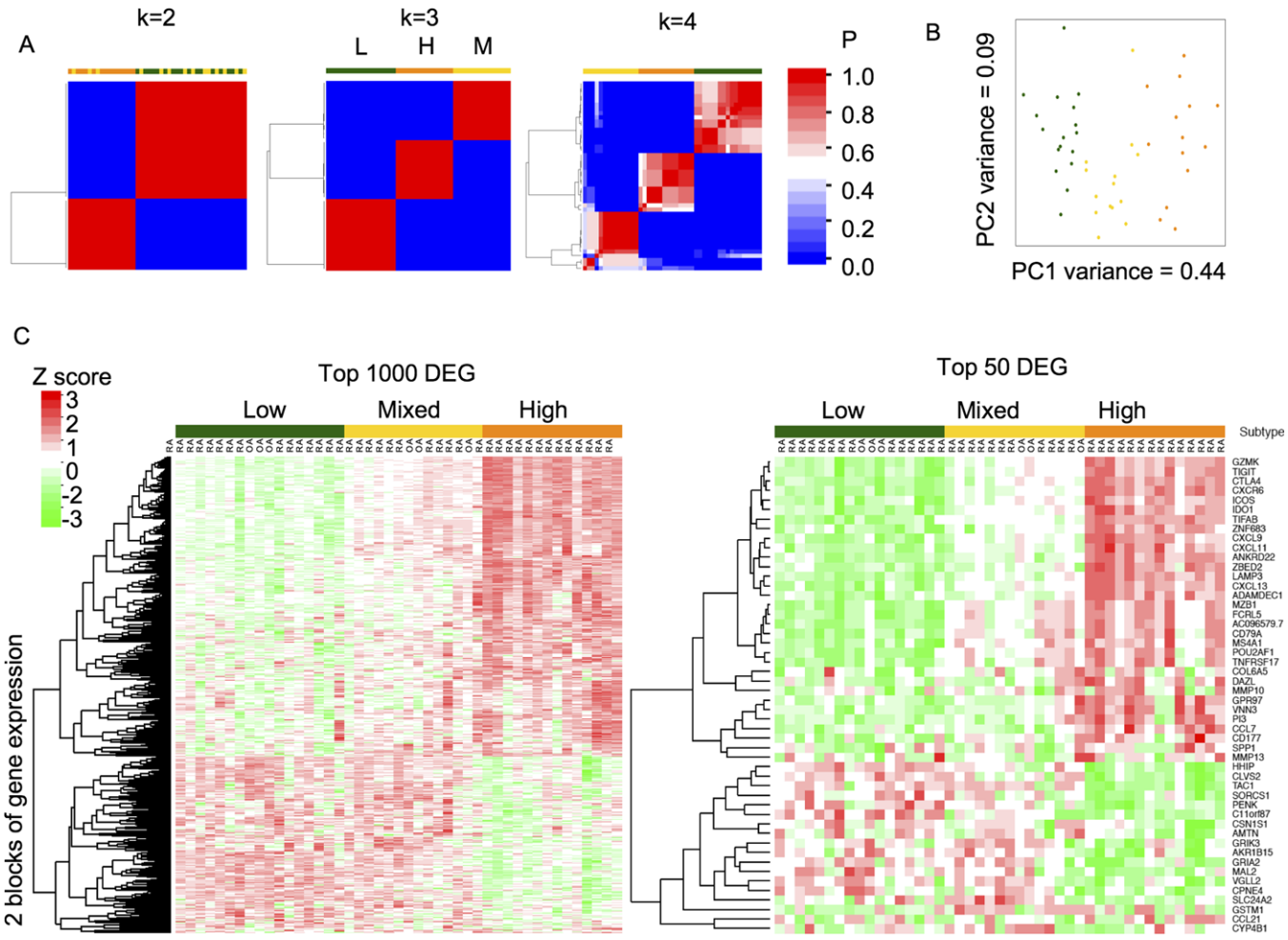

Figure 3. Identification of 3 distinct synovial subtypes by gene expression analysis of 45 synovial tissue samples. **A,** Consensus clustering heatmaps using the top 500 most variable genes show clusters constrained to k = 2, k = 3, and k = 4. Red denotes samples that clustered together consistently, blue denotes samples that never clustered together, and white denotes samples that showed inconsistent co-clustering. P represents the probability score for co-clustering of individual samples. Samples were labeled green (low inflammatory [L]), orange (high inflammatory [H]), and yellow (mixed [M]) according to partitioning obtained when constraining the clustering algorithm to k = 3 clusters. **B,** Principal components analysis (PCA) of RNA-seq data shows a PCA plot of the RNA-seq data in relation to the top 500 most variable genes. Samples are color-coded according to cluster as defined in **A**. **C,** Heatmaps of normalized gene expression of the top 1,000 and top 50 differentially expressed genes (DEGs) are shown across the 3 clusters (low, mixed, and high inflammatory). Red denotes increased gene expression (Z score), and green denotes decreased gene expression.

We also explored this analysis using differing numbers of variable genes (see Supplementary Figure 1, available on the *Arthritis & Rheumatology* web site at http://onlinelibrary.wiley.com/doi/10.1002/art.40428/abstract) and identified very minor shifts across the 3 consensus clustering subtypes, lending confidence to the k = 3 sample partitioning. Principal components analysis of the samples using the top 500 most variable genes demonstrated agreement with the findings from the RNA-seq analyses that revealed the 3 synovial subtypes (Figure 3B), thus validating the clustering analysis.

Differential gene expression patterns between the 3 synovial subtypes. We identified 6,582 transcripts as DEGs ($P_{adj} < 0.01$) across the 3 synovial clusters. Comparisons of each cluster to the others are presented in Supplementary Tables 2, 3, and 4 (available on the *Arthritis & Rheumatology* web site at http://onlinelibrary.wiley.com/doi/10.1002/art.40428/abstract). More than one-half of these DEGs separated the low inflammatory from the high inflammatory subtype, while the majority of the remaining genes separated the mixed from the high inflammatory subtype. The mixed subtype shares features with both the high and low inflammatory subtypes. Since it is a blend of the 2 subtypes, there are very few genes that are unique to the mixed group. Heatmaps of the top 1,000 and top 50 most variable genes (as ranked by DESeq2 analysis based on the P_{adj} value output) depict the main gene expression patterns segregating the 3 subtypes (Figure 3C). The largest gene block displayed an increasing expression pattern as the categories progressed from low to mixed to high inflammatory subtype (see Supplementary Table 5, available on the *Arthritis & Rheumatology* web site at http://onlinelibrary.wiley.com/doi/10.1002/art.40428/abstract).

Using DAVID gene ontology analysis, we performed functional annotation clustering on the genes with increased expression in the high inflammatory subtype compared to the others, and found that the highest enrichment scores corresponded to the pathways of immunity, immune cell signaling (such as SH2 and SH3 domains and kinases), and immunoglobulins, as well as chemokines and cytokines (Figure 4A) (see also

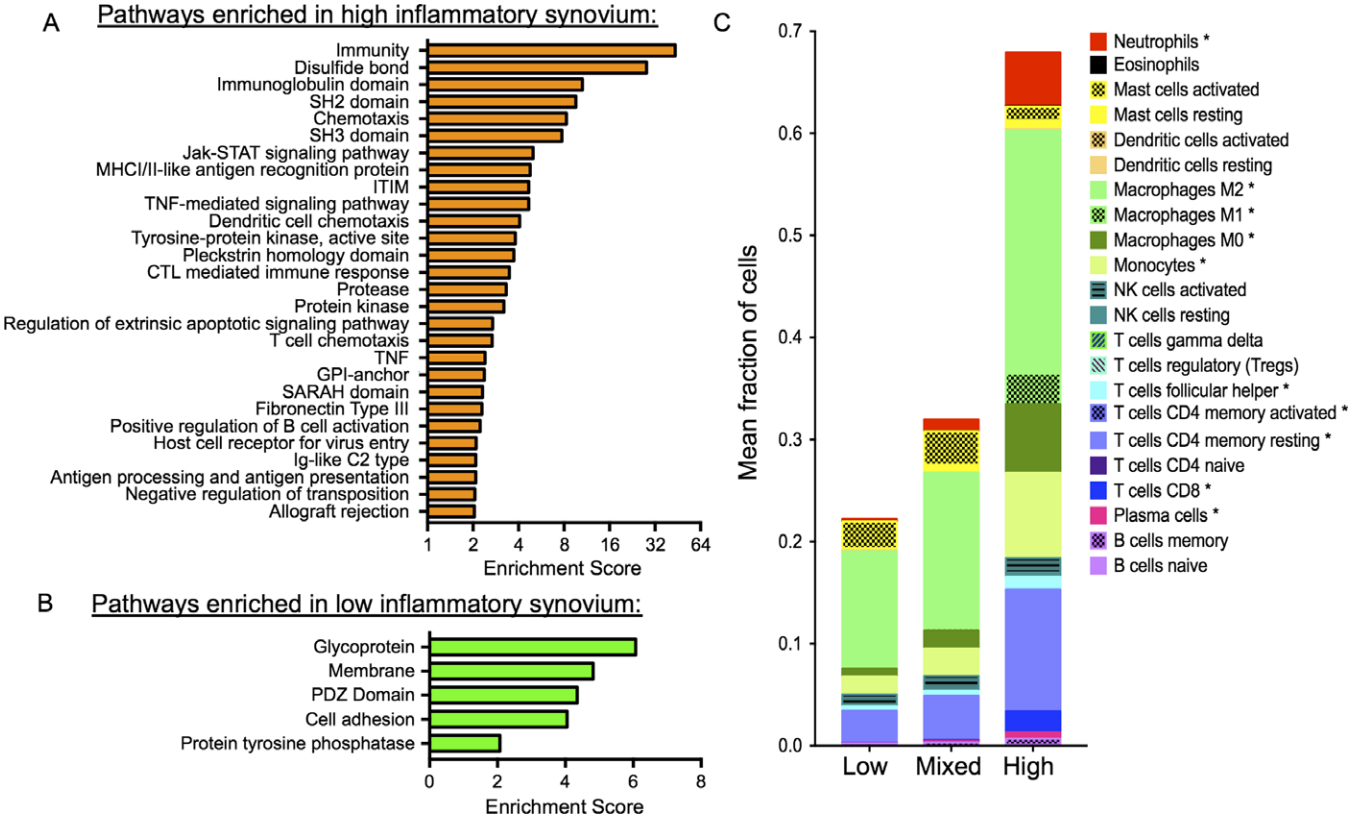

Figure 4. Gene expression characteristics of the 3 synovial subtypes. **A,** Enrichment scores of functional annotation clusters of genes with increased expression in the high inflammatory subtype compared to the other subtypes. **B,** Enrichment scores of functional annotation clusters of genes with increased expression in the low inflammatory subtype compared to the other subtypes. **C,** CIBERSORT-inferred fraction of leukocyte cell types according to the 3 synovial subtypes. * = $P < 0.05$, by Kruskal-Wallis test. MHCI/II = major histocompatibility complex class I/class II; ITIM = immunoreceptor tyrosine–based inhibition motif; TNF = tumor necrosis factor; CTL = cytotoxic T lymphocyte; GPI = glycoprotein I; NK = natural killer.

Supplementary Table 6, http://onlinelibrary.wiley.com/doi/10.1002/art.40428/abstract).

A smaller block of genes showed higher expression in the low inflammatory and mixed subtypes than in the high inflammatory subtype (Figure 3C) (see also Supplementary Table 7, http://onlinelibrary.wiley.com/doi/10.1002/art.40428/abstract). Functional annotation clustering of genes with increased expression in the low inflammatory subtype compared to the other subtypes identified enrichment in pathways that included glycoproteins (Figure 4B) (see also Supplementary Table 8, http://onlinelibrary.wiley.com/doi/10.1002/art.40428/abstract). These genes included markers of lining layer fibroblasts such as *CD55*, transforming growth factor β (TGFβ) superfamily genes (*TGFBR1, TGFBR2*, *TGFB2*, and *BMP6*), and genes involved in the regulation of extracellular glycoproteins such as *GCNT3* (a glycosyltransferase that mediates core *O*-glycan branching, a critical step in mucin synthesis) (26–30). Another enriched pathway in the low inflammatory subtype included cell adhesion (Figure 4B). This pathway includes protocadherin gamma genes, a family of cell-adhesion proteins predominantly expressed in neuronal synapses that are critical for axon targeting and neuron survival (31–34).

Other significantly enriched pathways were those involved in neuronal pain processing. For example, *ADRA1B* (α-1 adrenergic receptor) is up-regulated on nociceptive nerve fibers that survive peripheral injury (35–37). We also analyzed expression of genes previously identified to discriminate lymphoid, myeloid, fibroid, and low inflammatory synovial subtypes (5). Samples from our high inflammatory subtype demonstrated elevated expression of myeloid genes as well as lymphoid signature genes (see Supplementary Figure 2, http://onlinelibrary.wiley.com/doi/10.1002/art.40428/abstract). The previously described "fibroid" synovial subtype was enriched in TGFβ signaling pathway genes, with a relative paucity of inflammatory gene expression (5). We confirmed that these genes were also overexpressed in our low inflammatory subtype (Supplementary Figure 2).

CIBERSORT deconvolution of synovial gene expression subgroups. Identifying the cellular source of gene expression variation can be challenging in samples containing various cell types, due to differences both in proportions and in total cell quantities. To better characterize the cell types responsible for gene expression differences among the synovial tissue samples, we applied the machine learning framework of CIBERSORT to estimate cell type composition. We compared inferred leukocyte frequencies using CIBERSORT analysis of gene expression profiles across the 3 synovial subtypes. The clusters were characterized by a successive increase in the proportion of hematopoietic cells between the low (23%), mixed (32%) and high inflammatory (68%) subgroups (Figure 4C). The high inflammatory subgroup harbored significantly increased inferred fractions of neutrophils as well as M2, M1, and M0 macrophages, monocytes, T follicular helper cells, memory activated and resting CD4 T cells, CD8 T cells, and plasma cells.

Predicting gene expression subtypes from histologic features using machine learning. One of our main goals was to determine the synchrony between synovial histologic features and their genomic subtypes, the existence of which enables a cheaper histology-based approach to characterizing synovial tissue. To this end, we implemented a leave-one-out cross-validation SVM classification system to predict synovial genomic subtypes for our 45 samples, using a binary representation for the histologic scores as training features and genomic subtypes as training labels for the model. The predictive power of this system was evaluated by measuring the area under the receiver operating characteristic curve (AUC) (Figure 5A). Models separating the high inflammatory subtype from the others and those separating the low inflammatory subtype from the others performed best (AUCs of 0.88 and 0.71, respectively), whereas models separating the mixed subtype from the others were harder to predict (AUC of 0.59).

We compared the predicted synovial subtypes to those assigned by RNA-seq clustering, and found agreement with the RNA-seq data in 39 of the 45 samples. Histologic feature weights were extracted from the modeling system (as shown in Figure 5B), and we observed that, in general, the most discriminatory features also had stronger interrater reliability (Figure 2B).

After observing satisfactory training and testing results across the 45 RNA-seq samples, we computed 2 SVMs using all 45 samples: one SVM was used to discriminate the low inflammatory subtype from the others, and one was used to discriminate the high inflammatory subtype from the others. We used these models to predict genomic subtypes of the remaining 82 synovial samples for which we had complete histologic and clinical laboratory data available, but not gene expression data. We compared the distributions of histologic features across the RNA-seq samples from 39 RA patients classified by gene expression clustering to the distributions of histologic features across the 82 samples classified by the histologic scoring algorithm. The distributions of histologic features were similar whether the samples were classified by gene expression clusters or by the histologic feature algorithm (Figure 5C). For example, lymphocyte scores were always highest in the high inflammatory subtype, regardless of how the subtypes

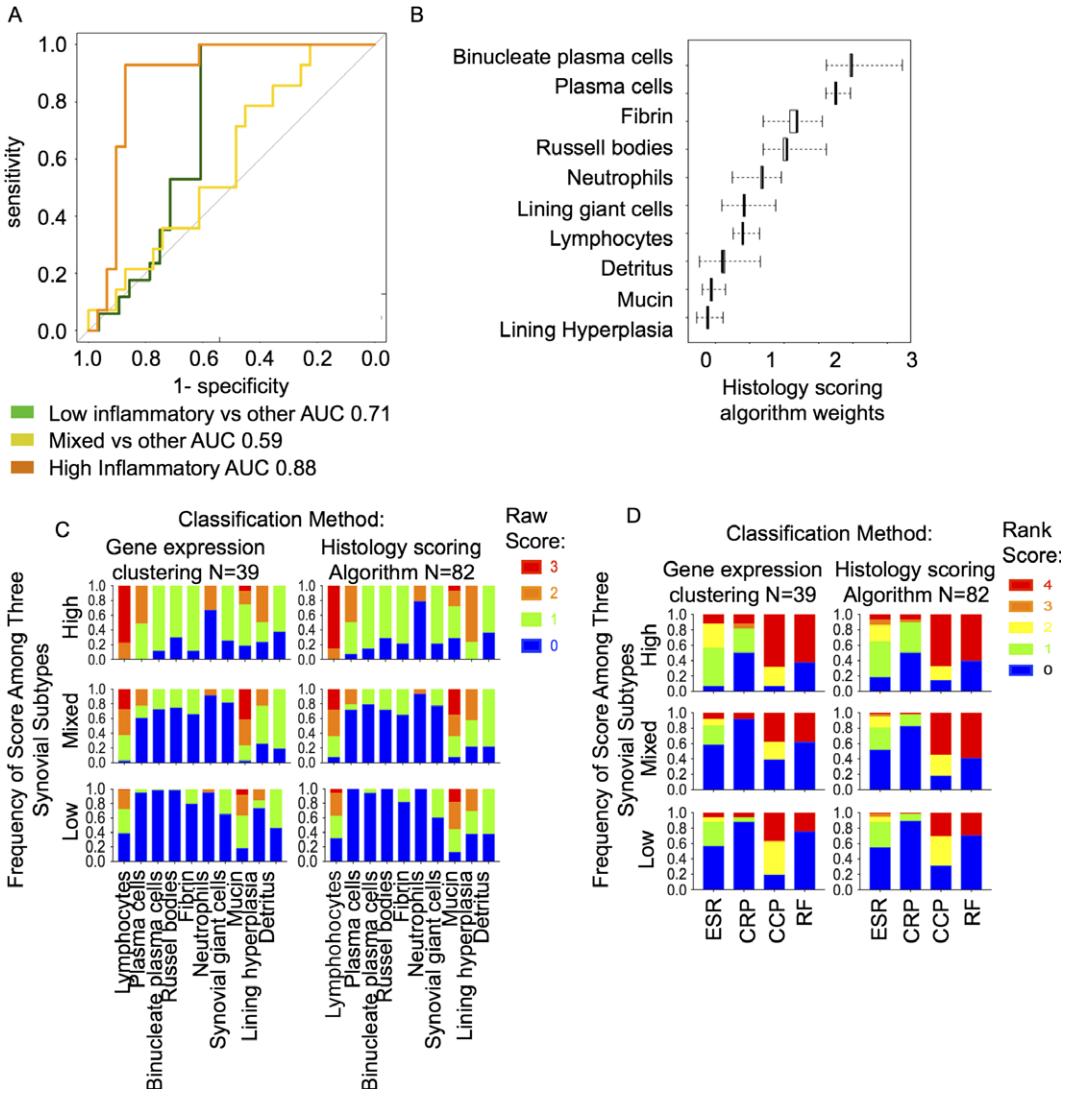

Figure 5. Machine learning classification of histologic features using RNA-seq–defined synovial subgroups. **A,** Receiver operating characteristic curves (ROCs) for the histologic scoring algorithm, with area under the ROC (AUC) for the 3 synovial subtypes. **B,** Mean absolute weights for 10 histologic features, showing separation of the high inflammatory subtype from the other subtypes classified by the histologic scoring algorithm. Results are the median (interquartile range). **C,** Frequency distribution of raw histologic scores among the 3 synovial subtypes in rheumatoid arthritis (RA) patients, classified by either RNA-seq clustering (left) or histologic scoring algorithm (right). **D,** Frequency distribution of clinical laboratory features in RA patients (rank score: 0 = minimum, 1 = 25th percentile, 2 = 50th percentile, 3 = 75th percentile, 4 = maximum) among the 3 synovial subtypes classified by either gene expression clustering (left) or histologic scoring algorithm (right). ESR = erythrocyte sedimentation rate; CRP = C-reactive protein; CCP = anti–cyclic citrullinated peptide antibodies; RF = rheumatoid factor.

were classified. This is an expected result and serves to validate our approach.

We also compared the distributions of clinical laboratory features between the 39 RA patients classified by gene expression clusters and the 82 RA patients classified by the histologic scoring algorithm (Figure 5D), and again found consistent patterns. Given that clinical features were not part of the development of the algorithm, this consistent distribution of clinical features demonstrates that both classification methods showed associations in meaningful ways with clinical laboratory features. For example, low ESR values were most commonly present in the low inflammatory subtype and rarely present in the high inflammatory subtype, whether classified by gene expression or the histologic scoring algorithm. This consistent partitioning of an independent set of clinical features provides additional confirmation for the histologic scoring algorithm.

Association of synovial subtypes with clinical features. We next compared the clinical features of all 123 RA patients who were classified using the histologic scoring algorithm. First, we compared the histologic features across the 3 subtypes and found that the levels of lymphocytes, plasma cells, synovial lining hyperplasia,

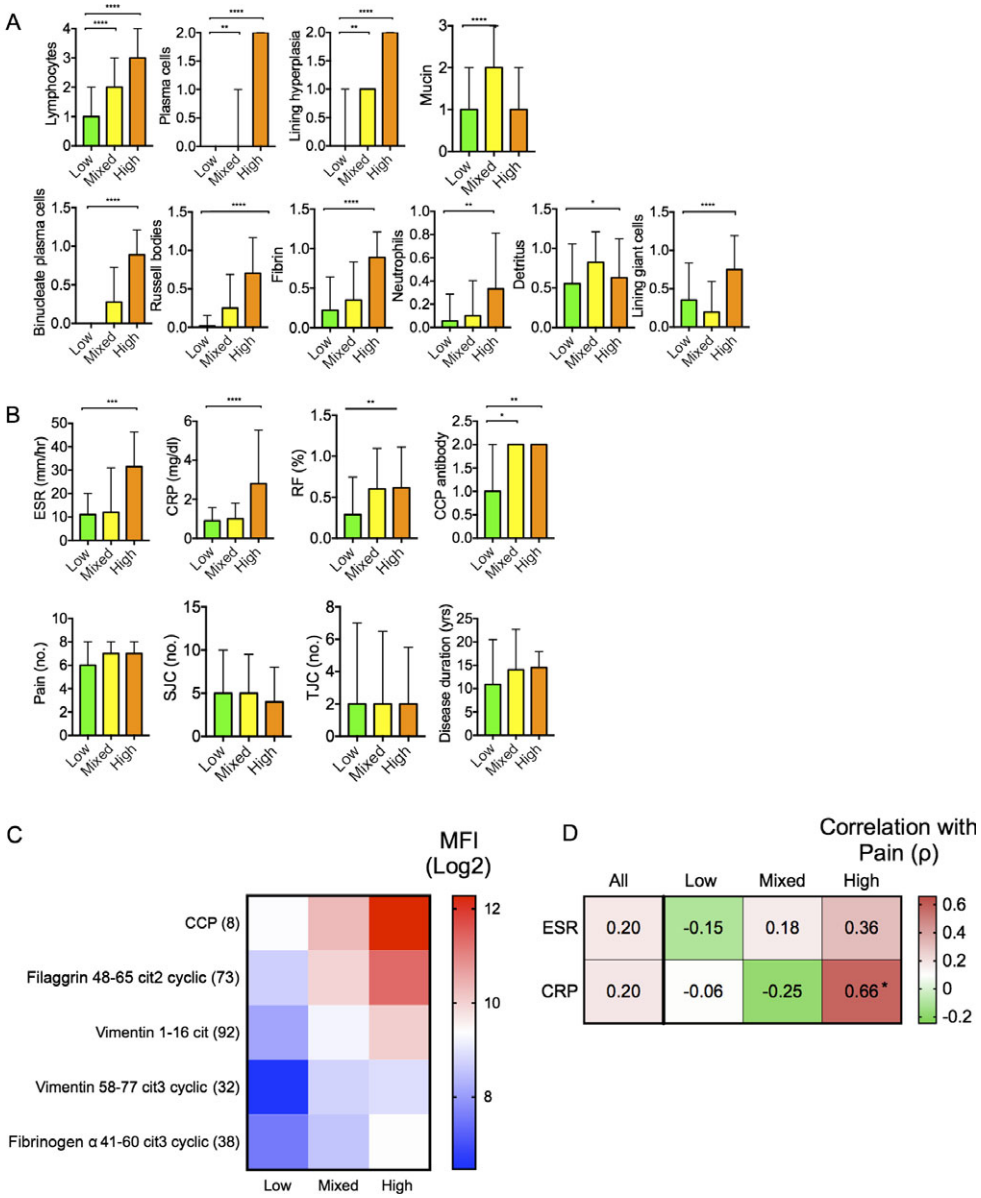

Figure 6. Comparison of clinical and histologic features in 123 patients with rheumatoid arthritis (RA) classified by synovial subtype according to the histologic scoring algorithm. **A,** Histologic scores of various features identified in RA patients in the low, mixed, and high inflammatory subtypes. Top, Ordinal features; scores are the median (interquartile range). Bottom, Binary features; scores are the mean ± SD. Top, ** = $P < 0.01$; **** = $P < 0.0001$, by Kruskal-Wallis test with Dunn's test for multiple comparisons. Bottom, * = $P < 0.05$; ** = $P < 0.01$; **** = $P < 0.0001$, by chi-square test. **B,** Clinical features of the RA patients in the low, mixed, and high inflammatory subtypes. Values are the median (interquartile range). * = $P < 0.05$; ** = $P < 0.01$; *** = $P < 0.001$; **** = $P < 0.0001$, by Kruskal-Wallis test with Dunn's test for multiple comparisons. **C,** Log_2-transformed plasma levels of antibodies to putative RA-associated autoantigens. Results are the mean fluorescence intensity (MFI). Antibody levels were significantly different among the 3 synovial subtypes, as determined by analysis of variance with Tukey's test for multiple comparisons. Values in parentheses are the number of samples from patients assigned to each synovial subtype. **D,** Spearman's correlation (rho) coefficients for the assessment of correlations between pain severity scores and levels of acute-phase reactants (erythrocyte sedimentation rate [ESR] and C-reactive protein [CRP]) across the 3 synovial subtypes. RF = rheumatoid factor; CCP = anti–cyclic citrullinated peptide antibodies; SJC = swollen joint count; TJC = tender joint count.

binucleated plasma cells, Russell bodies, fibrin, and neutrophils were all significantly increased in the high inflammatory samples (Figure 6A). These findings were consistent with the observed fractions of cells inferred from the gene expression data (Figure 4C). Similarly, the ESR and the levels of CRP, RF, and anti-CCP were increased in patients with high inflammatory scores (Figure 6B).

We also compared the fine specificity of ACPAs between the synovial subtypes (see Supplementary Figure 3, http://onlinelibrary.wiley.com/doi/10.1002/art.40428/abstract), and identified significantly increased levels of autoantibodies to citrullinated filaggrin, vimentin, and fibrinogen α peptides in patients in the high inflammatory subgroup (Figure 6C). Unexpectedly, these subtype differences were not observed when compared according to clinical assessments of pain, tender joint counts, swollen joint counts, or disease duration (Figure 6B). Patients in the low inflammatory subtype had high pain severity scores (median pain score of 6 on a scale of 1–10) but little inflammation in the tissue (according to gene expression data, histologic assessments, or levels of systemic inflammation markers in the blood [i.e., ESR and CRP levels).

We therefore hypothesized that pain might be driven by distinct mechanisms in the various synovial subtypes. To explore this hypothesis, we compared the Spearman's rank correlation coefficients between the levels of acute-phase reactants and pain scores across all synovial samples grouped together and when parsed according to patient synovial histologic subtype. We found a weak, nonsignificant correlation between pain scores and levels of acute-phase reactants when all patients were analyzed together (Figure 6D), and this became more clear when we divided the patients according to synovial histologic subtype. Patients with high inflammatory synovium, but not those with the other synovial subtypes, showed a stronger, significant correlation between pain scores and CRP levels. This suggests that pain is associated with inflammation in patients with the high inflammatory subtype, and that pain may be driven by distinct mechanisms in the other patients.

DISCUSSION

After we identified 3 synovial gene expression subtypes in RA and OA patients, we developed a histology machine learning model trained on these subtypes, predicting genomic subtypes from histologic data. Through our modeling system, we found that the histologic features that most strongly defined the high inflammatory subtype included 3 plasma cell features: binucleated plasma cells, percentages of plasma cells, and Russell bodies (Figure 5B). Deconvolution of gene expression profiles indicated that the histologic scores of these plasma cell features on H&E-stained synovial samples were a harbinger of a leukocyte panoply that included T follicular helper cells, memory resting and activated CD4 T cells, CD8 T cells, monocytes, M0, M1, and M2 macrophages, and neutrophils. Our gene expression analysis did not identify distinct myeloid and lymphoid synovial histologic subtypes, in contrast to that observed in a previous study (5). It is possible that differences in the patient populations or treatments could account for those discrepant results.

Analysis of the low inflammatory subtype identified expression of genes involved in glycoprotein production and TGFβ pathways (fibroid genes), as well as neuronal genes. This discovery is consistent with the results of at least one other prior study in which overexpression of neurogenesis pathway genes was identified in a low inflammatory subtype of RA (38). A common theme among the neuronal genes in this cluster is that they play a role in a maladaptive response of the nervous system to damage. It is interesting that this subtype is characterized by a paucity of inflammatory infiltrates, and yet high pain severity scores are maintained and multiple tender/swollen joints are present—this too is consistent with other findings in patients with established RA (39). Although it is possible that these patients had OA in the joint subjected to arthroplasty and had active RA in other joints, given the minimal amount of systemic and synovial inflammation, it raises the question as to whether the other joints might be perceived (by the evaluating rheumatologist) as being tender and swollen potentially as a result of mechanisms other than inflammation. For example, synovial proteoglycans such as mucin, which was common in the synovial samples, has a jelly-like consistency and could be perceived by the evaluating clinician as synovial swelling. Similarly, tenderness and pain could be attributable to noninflammatory mechanisms, and this is consistent with the dissociation of pain scores from levels of systemic inflammation markers (Figure 6D) as well as the enrichment for neuronal gene expression (Figure 4B) in the low inflammatory and mixed synovial subtypes.

Our findings suggest that in RA patients with longstanding disease who exhibit a poor response to antiinflammatory treatment, synovial biopsy may be warranted to determine their inflammatory subtype. Better understanding of the cause of pain in patients with little tissue inflammation is critical, because pain not attributable to inflammation and mucin-related synovial thickening could result in high tender and swollen joint counts in the absence of systemic inflammation (low ESR and CRP levels). We would expect such

patients to respond poorly to antirheumatic drugs that target inflammation.

Several important limitations of this study should be noted. The lack of normal synovium tissue samples makes it challenging to draw conclusions about the genes overexpressed in the low inflammatory subtype. These genes could represent a pathologic process or simply represent relative enrichment of normal resident cells. Another challenge in interpreting these results is that the cell bodies of sensory neurons reside in the dorsal root ganglion and are not captured when sampling synovial tissue. It is possible that synaptic mRNA (40) from damaged nerve fibers were captured in our tissue samples, or that resident synovial cells express a broad array of neural genes in response to inflammation. For example, synovial fibroblasts have been shown to express α7 nicotinic receptor (41) and substance P (42).

Another limitation of this work is that our tissue samples were dissociated into single-cell suspensions prior to RNA fixation. Based on the significant numbers of plasma cells counted by histologic assessment, it is likely that the CIBERSORT-inferred frequencies of plasma cells were lower than those observed with H&E staining, due to the fragility of plasma cells and occurrence of cell death during processing. Additional processing artifacts include immune cell activation due to various factors during dissociation. CIBERSORT was trained on microarray data and can only detect 22 potential cell types, so it is quite possible that other cell types, such as plasmablasts and peripheral helper T cells (43), are present but are not annotated by CIBERSORT.

Yet one other limitation in this project is that the machine learning model was trained and tested on just 45 synovial samples—a larger data set would offer more statistical power, and we plan to run more samples in the future. Finally, the cohort studied had longstanding disease and had been exposed to various treatments. Further assessment of small joint tissue from patients with early RA would be useful to characterize features important for the understanding of RA pathogenesis and for predicting treatment responses.

In summary, machine learning integration and analysis of histologic and transcriptional data sets identified 3 distinct molecular subtypes of RA that correlated with specific clinical phenotypes. The high inflammatory subtype is associated with high levels of synovial and systemic inflammation and autoantibodies. The low inflammatory subgroup is characterized by high neuronal and glycoprotein gene expression, as well as pain severity scores that are dissociated from the elevated levels of systemic inflammation markers.

ACKNOWLEDGMENT

We would like to thank Nathalie Blachere for providing editorial assistance. The RNA-seq data set and histologic scores can be accessed at the ImmPort repository (accession no. SDY1299), available at https://www.immport-open/public/study/displayStudyDetail/SDY1299.

AUTHOR CONTRIBUTIONS

All authors were involved in drafting the article or revising it critically for important intellectual content, and all authors approved the final version to be published. Dr. Orange had full access to all of the data in the study and takes responsibility for the integrity of the data and the accuracy of the data analysis.

Study conception and design. Orange, Agius, DiCarlo, Figgie, Ivashkiv, Pernis, Bykerk, Goodman, Donlin.

Acquisition of data. Orange, Agius, DiCarlo, McNamara, Cummings, Andersen, Mirza, Lingampali, Bykerk, Goodman, Donlin.

Analysis and interpretation of data. Orange, Agius, DiCarlo, Robine, Geiger, Szymonifka, Figgie, Jiang, Frank, Darnell, Robinson, Gravallese, Bykerk, Goodman, Donlin.

REFERENCES

1. Pitzalis C, Kelly S, Humby F. New learnings on the pathophysiology of RA from synovial biopsies. Curr Opin Rheumatol 2013;25:334–44.
2. De Groof A, Ducreux J, Humby F, Nzeusseu Toukap A, Badot V, Pitzalis C, et al. Higher expression of TNFα-induced genes in the synovium of patients with early rheumatoid arthritis correlates with disease activity, and predicts absence of response to first line therapy. Arthritis Res Ther 2016;18:19.
3. Hogan VE, Holweg CT, Choy DF, Kummerfeld SK, Hackney JA, Teng YK, et al. Pretreatment synovial transcriptional profile is associated with early and late clinical response in rheumatoid arthritis patients treated with rituximab. Ann Rheum Dis 2012;71:1888–94.
4. Klaasen R, Thurlings RM, Wijbrandts CA, van Kuijk AW, Baeten D, Gerlag DM, et al. The relationship between synovial lymphocyte aggregates and the clinical response to infliximab in rheumatoid arthritis: a prospective study. Arthritis Rheum 2009;60:3217–24.
5. Dennis G Jr, Holweg CT, Kummerfeld SK, Choy DF, Setiadi AF, Hackney JA, et al. Synovial phenotypes in rheumatoid arthritis correlate with response to biologic therapeutics. Arthritis Res Ther 2014;16:R90.
6. Smolen JS, Landewé R, Bijlsma J, Burmester G, Chatzidionysiou K, Dougados M, et al. EULAR recommendations for the management of rheumatoid arthritis with synthetic and biological disease-modifying antirheumatic drugs: 2016 update. Ann Rheum Dis 2017;76:960–77.
7. Krenn V, Kurz B, Krukemeyer MG, Knoess P, Jakobs M, Poremba C, et al. Histopathological degeneration score of fibrous cartilage: low- and high-grade meniscal degeneration. Z Rheumatol 2010;69:644–52. In German.
8. Krenn V, Morawietz L, König B, Otto M, Kriegsmann J, Köpenik A, et al. Low-grade-/high-grade-synovitis: synovitis-score as a gold standard? Orthopade 2006;35:853–9. In German.
9. Slansky E, Li J, Häupl T, Morawietz L, Krenn V, Pessler F. Quantitative determination of the diagnostic accuracy of the synovitis score and its components. Histopathology 2010;57:436–43.
10. Pearle AD, Scanzello CR, George S, Mandl LA, DiCarlo EF, Peterson M, et al. Elevated high-sensitivity C-reactive protein levels are associated with local inflammatory findings in patients with osteoarthritis. Osteoarthritis Cartilage 2007;15:516–23.
11. Thurlings RM, Wijbrandts CA, Mebius RE, Cantaert T, Dinant HJ, van der Pouw-Kraan TC, et al. Synovial lymphoid neogenesis

does not define a specific clinical rheumatoid arthritis phenotype. Arthritis Rheum 2008;58:1582–9.
12. Prieto-Potin I, Largo R, Roman-Blas JA, Herrero-Beaumont G, Walsh DA. Characterization of multinucleated giant cells in synovium and subchondral bone in knee osteoarthritis and rheumatoid arthritis. BMC Musculoskelet Disord 2015;16:226.
13. Riddle JM, Bluhm GB, Barnhart MI. Interrelationships between fibrin, neutrophils and rheumatoid synovitis. J Reticuloendothel Soc 1965;2:420–36.
14. Orlovskaya GV, Muldiyarov PY, Kazakova IS. Synovial plasma cells in rheumatoid arthritis: electron microscope and immunofluorescence studies. Ann Rheum Dis 1970;29:524–32.
15. Perry ME, Mustafa Y, Wood SK, Cawley MI, Dumonde DC, Brown KA. Binucleated and multinucleated forms of plasma cells in synovia from patients with rheumatoid arthritis. Rheumatol Int 1997;17:169–74.
16. Volin MV, Shahrara S, Haines GK III, Woods JM, Koch AE. Expression of mucin 3 and mucin 5AC in arthritic synovial tissue. Arthritis Rheum 2008;58:46–52.
17. Revell PA, Mayston V, Lalor P, Mapp P. The synovial membrane in osteoarthritis: a histological study including the characterisation of the cellular infiltrate present in inflammatory osteoarthritis using monoclonal antibodies. Ann Rheum Dis 1988;47:300–7.
18. Aletaha D, Neogi T, Silman AJ, Funovits J, Felson DT, Bingham CO III, et al. 2010 rheumatoid arthritis classification criteria: an American College of Rheumatology/European League Against Rheumatism collaborative initiative. Arthritis Rheum 2010;62:2569–81.
19. Arnett FC, Edworthy SM, Bloch DA, McShane DJ, Fries JF, Cooper NS, et al. The American Rheumatism Association 1987 revised criteria for the classification of rheumatoid arthritis. Arthritis Rheum 1988;31:315–24.
20. Dobin A, Davis CA, Schlesinger F, Drenkow J, Zaleski C, Jha S, et al. STAR: ultrafast universal RNA-seq aligner. Bioinformatics 2013;29:15–21.
21. Leek JT, Storey JD. Capturing heterogeneity in gene expression studies by surrogate variable analysis. PLoS Genet 2007;3:1724–35.
22. Love MI, Huber W, Anders S. Moderated estimation of fold change and dispersion for RNA-seq data with DESeq2. Genome Biol 2014;15:550.
23. Dennis G Jr, Sherman BT, Hosack DA, Yang J, Gao W, Lane HC, et al. DAVID: Database for Annotation, Visualization, and Integrated Discovery. Genome Biol 2003;4:P3.
24. Sokolove J, Bromberg R, Deane KD, Lahey LJ, Derber LA, Chandra PE, et al. Autoantibody epitope spreading in the preclinical phase predicts progression to rheumatoid arthritis. PLoS One 2012;7:e35296.
25. McHugh ML. Interrater reliability: the kappa statistic. Biochem Med (Zagreb) 2012;22:276–82.
26. Palmer DG, Selvendran Y, Allen C, Revell PA, Hogg N. Features of synovial membrane identified with monoclonal antibodies. Clin Exp Immunol 1985;59:529–38.
27. Smith MD, Barg E, Weedon H, Papengelis V, Smeets T, Tak PP, et al. Microarchitecture and protective mechanisms in synovial tissue from clinically and arthroscopically normal knee joints. Ann Rheum Dis 2003;62:303–7.
28. Yeh JC, Ong E, Fukuda M. Molecular cloning and expression of a novel β-1, 6-N-acetylglucosaminyltransferase that forms core 2, core 4, and I branches. J Biol Chem 1999;274:3215–21.
29. Mizoguchi F, Slowikowski K, Wei K, Marshall JL, Rao DA, Kyung Chang S, et al. Functionally distinct disease-associated fibroblast subsets in rheumatoid arthritis. Nature Communications 2018;9:789.
30. Stephenson W, Donlin LT, Butler A, Rozo C, Bracken B, Rashidfarrokhi A, et al. Single-cell RNA-seq of rheumatoid arthritis synovial tissue using low-cost microfluidic instrumentation. Nature Communications 2018;9:791.
31. Leung LC, Urbančič V, Baudet ML, Dwivedy A, Bayley TG, Lee AC, et al. Coupling of NF-protocadherin signaling to axon guidance by cue-induced translation. Nat Neurosci 2013;16:166–73.
32. Hasegawa S, Kumagai M, Hagihara M, Nishimaru H, Hirano K, Kaneko R, et al. Distinct and cooperative functions for the protocadherin-α, -β and -γ clusters in neuronal survival and axon targeting. Front Mol Neurosci 2016;9:155.
33. Junghans D, Heidenreich M, Hack I, Taylor V, Frotscher M, Kemler R. Postsynaptic and differential localization to neuronal subtypes of protocadherin β16 in the mammalian central nervous system. Eur J Neurosci 2008;27:559–71.
34. Asahina H, Masuba A, Hirano S, Yuri K. Distribution of protocadherin 9 protein in the developing mouse nervous system. Neuroscience 2012;225:88–104.
35. Drummond ES, Dawson LF, Finch PM, Bennett GJ, Drummond PD. Increased expression of cutaneous α1-adrenoceptors after chronic constriction injury in rats. J Pain 2014;15:188–96.
36. Drummond PD, Drummond ES, Dawson LF, Mitchell V, Finch PM, Vaughan CW, et al. Upregulation of α1-adrenoceptors on cutaneous nerve fibres after partial sciatic nerve ligation and in complex regional pain syndrome type II. Pain 2014;155:606–16.
37. Lee YH, Ryu TG, Park SJ, Yang EJ, Jeon BH, Hur GM, et al. α1-adrenoceptors involvement in painful diabetic neuropathy: a role in allodynia. Neuroreport 2000;11:1417–20.
38. Van Baarsen LG, Wijbrandts CA, Timmer TC, van der Pouw Kraan TC, Tak PP, Verweij CL. Synovial tissue heterogeneity in rheumatoid arthritis in relation to disease activity and biomarkers in peripheral blood. Arthritis Rheum 2010;62:1602–7.
39. Horton SC, Walsh CA, Emery P. Established rheumatoid arthritis: rationale for best practice: physicians' perspective of how to realise tight control in clinical practice. Best Pract Res Clin Rheumatol 2011;25:509–21.
40. Meer EJ, Wang DO, Kim S, Barr I, Guo F, Martin KC. Identification of a cis-acting element that localizes mRNA to synapses. Proc Natl Acad Sci U S A 2012;109:4639–44.
41. Waldburger JM, Boyle DL, Pavlov VA, Tracey KJ, Firestein GS. Acetylcholine regulation of synoviocyte cytokine expression by the α7 nicotinic receptor. Arthritis Rheum 2008;58:3439–49.
42. Inoue H, Shimoyama Y, Hirabayashi K, Kajigaya H, Yamamoto S, Oda H, et al. Production of neuropeptide substance P by synovial fibroblasts from patients with rheumatoid arthritis and osteoarthritis. Neurosci Lett 2001;303:149–52.
43. Rao DA, Gurish MF, Marshall JL, Slowikowski K, Fonseka CY, Liu Y, et al. Pathologically expanded peripheral T helper cell subset drives B cells in rheumatoid arthritis. Nature 2017;542:110–4.